



1 **Impact of the Green Light Program on haze pollution in**  
2 **the North China Plain, China**

3 Xin Long<sup>1,3,7</sup>, Xuexi Tie<sup>1,2,3,4,5\*</sup>, Jiamao Zhou<sup>3</sup>, Wenting Dai<sup>3</sup>, Xueke Li<sup>6</sup>, Tian  
4 Feng<sup>1</sup>, Guohui Li<sup>1,3</sup>, Junji Cao<sup>1,3</sup>, and Zhisheng An<sup>1</sup>

5 <sup>1</sup>State Key Laboratory of Loess and Quaternary Geology, SKLLQG, Institute of Earth  
6 Environment, Chinese Academy of Sciences, Xi'an 710061, China

7 <sup>2</sup>Center for Excellence in Urban Atmospheric Environment, Institute of Urban Environment,  
8 Chinese Academy of Sciences, Xiamen 361021, China

9 <sup>3</sup>Key Laboratory of Aerosol Chemistry and Physics, Institute of Earth Environment, Chinese  
10 Academy of Sciences, Xi'an 710061, China

11 <sup>4</sup>Shanghai Key Laboratory of Meteorology and Health, Shanghai, 200030, China

12 <sup>5</sup>National Center for Atmospheric Research, Boulder, CO 80303, USA

13 <sup>6</sup>Department of Geography, University of Connecticut, Storrs, Mansfield, CT 06269, USA

14 <sup>7</sup>School of Environment Science and Engineering, Southern University of Science and  
15 Technology, Shenzhen 518055, China

16

17 *Correspondence to:* Xuexi Tie (email: [xxtie@ucar.edu](mailto:xxtie@ucar.edu))

18



19 **Abstract.** As the world's largest developing country, China undergoes the ever-increasing  
20 demand for electricity during the past few decades. In 1996, China launched the Green Lights  
21 Program (GLP), which becomes a national energy conservation activity for saving lighting  
22 electricity, as well as an effective reduction of the coal consumption for power generation.  
23 Despite of the great success of the GLP, its effects on haze pollution have not been  
24 investigated and well understood. This study focused to assess the potential coal-saving  
25 induced by the GLP and to estimate the consequent improvements of the haze pollutions in the  
26 North China Plain (NCP), because severe haze pollutions often occur in the NCP and a large  
27 amount of power plants locate in this region. The estimated potential coal-saving induced by  
28 the GLP can reach a massive value of 120–323 million tons, accounting for 6.7–18.0% of the  
29 total coal consumption for thermal power generation in China. In December 2015, there was a  
30 massive potential emission reduction of air pollutants from thermal power generation in the  
31 NCP, which was estimated to be 20.0–53.8 Gg for NO<sub>x</sub> and 6.9–18.7 Gg for SO<sub>2</sub>. The  
32 potential emission reductions induced by the GLP played important roles in the haze formation,  
33 because the NO<sub>x</sub> and SO<sub>2</sub> are important precursors for the formation of particles. To assess the  
34 impact of the GLP on haze pollution, sensitive studies were conducted by applying a regional  
35 chemical/dynamical model (WRF-CHEM). The model results suggest that in the lower limit  
36 case of emission reduction, the PM<sub>2.5</sub> concentration decreases by 2–5 μg m<sup>-3</sup> in large areas of  
37 the NCP. In the upper limit case of emission reduction, there was much more remarkable  
38 decrease in PM<sub>2.5</sub> concentration (4–10 μg m<sup>-3</sup>). This study is a good example to illustrate that  
39 scientific innovation can induce important benefits on environment issues, such as haze  
40 pollution.

41

42 **Keywords:** Green Light Programs; thermal power plants; Haze in NCP; WRF-CHEM



## 43 **1 Introduction**

44 As the world's largest developing country, China undergoes the ever-increasing demand for  
45 electricity during the past few decades. Artificial lighting is an important part of China's  
46 energy consumption, accounting for a quite stable share of about 10–14% of the total  
47 electricity consumption (Lv and Lv, 2012; Zheng et al., 2016). Also, the lighting demand in  
48 China is predicted to increase continuously, with a projected average annual growth rate of 4.3%  
49 from 2002 to 2020 (Liu, 2009). With principal objective of alleviating shortage of electricity,  
50 China has launched the Green Lights Program (GLP) in 1996, with the core of aiming at  
51 replacing low-efficiency lighting lamps by high-efficiency ones. Since then, the GLP has  
52 become a national energy conservation activity for saving lighting electricity, and has been  
53 highlighted continuously in the nation's 9<sup>th</sup>–12<sup>th</sup> Five-Year Plan (1996–2015) (Lin, 1999).  
54 With the object of providing high-quality efficient lighting products, the GLP is undoubtedly a  
55 useful electricity-saving measurement. Nonetheless, driven by the accelerated economic  
56 increase, the thermal power electricity has experienced an ever-increasing trend in the past  
57 decades, as well as the associated coal consumption for thermal power generation. Thermal  
58 power generation is the primary electricity source in China, contributing to about 72–78% out  
59 of the total electricity (NBS, 2000–2016). In 2015, the coal consumption for thermal power  
60 generation in China raise to a very massive value of about 1.8 billion tons, which is 3.2 times  
61 of that in 2000. Simultaneously, the coal consumption for thermal power generation is 2.7  
62 times of that in the USA in 2015, which is reported to be 670 million tons  
63 (<https://www.eia.gov/totalenergy/data/browser/>, last accessed on 20 December, 2018).  
64 Due to the significant use of coal, thermal power generation is one of the dominant emission  
65 contributors to anthropogenic air pollutants in China (Tie and Cao, 2010; Wang and Hao, 2012;



66 Wang et al., 2015b). The power sector contributes significantly to air pollutants of the nitrogen  
67 oxides (NO<sub>x</sub>), the sulfur dioxide (SO<sub>2</sub>), and the particulate matter (PM) (Zhao et al., 2013;  
68 Huang et al., 2016). The pollutants of SO<sub>2</sub> and NO<sub>x</sub> are the precursors of secondary pollutant  
69 of ozone (O<sub>3</sub>), and secondary aerosols (Seinfeld et al., 1998; Laurent et al., 2014). It is also  
70 reported that emission from power sector is a major contributor to particulate sulfate, and  
71 nitrate (Zhang et al., 2012). The emissions from thermal power generation in China can also  
72 transport to a long distance, causing regional/global air pollutions (Tie et al., 2001; Huang et  
73 al., 2016). Considering the important contributions to air pollutants, controlling emissions from  
74 thermal power generation is a vital strategy for the improvement of air quality in China.

75 Distinguished from the ever-increasing trend of thermal power electricity and associated coal  
76 consumption, the increase trends of SO<sub>2</sub> and NO<sub>x</sub> emissions from thermal power generation  
77 are curbed and even change to decrease (Liu et al., 2015). This is caused by the famous  
78 nation-wide project of utilizing emission control facilities during 2005 to 2015, such as  
79 installing flue-gas desulfurization/denitrification systems and optimizing the generation fleet  
80 mix (Liu et al., 2015; Huang et al., 2016). Given the technological changes that have occurred  
81 in the power sector, the air pollutant emissions from power generation have been significantly  
82 reduced. However, the thermal power generation is still identified to be with massive air  
83 pollutant emissions, involving 5.1 million tons of NO<sub>x</sub>, 4.0 million tons for SO<sub>2</sub>, and 0.8  
84 millions tons of PM in 2015. Under high standards of ultra-low emission power units, the  
85 staggering total amount of coal consumption becomes a vital challenge for emission control  
86 from thermal power generation.

87 With ambitious and comprehensive efforts, the success of the GLP resulted in about 59 billion  
88 kWh of accumulated electricity savings from 1996 to 2005 (SCIO, 2006), and about 14.4



89 billion kWh of annual electricity savings from 2006 to 2010 (Lv and Lv, 2012). It is reported  
90 that the GLP has produced climate benefit for environment, reducing 17 million tons of CO<sub>2</sub>  
91 and 530 thousand tons of SO<sub>2</sub> emissions from 1996 to 2005 (Guo and Pachauri, 2017).  
92 Coordinate with the effectiveness of the GLP on energy saving, the effects of power generation  
93 or coal-saving on air quality are elaborated in previous studies (Liu et al., 2015; Huang et al.,  
94 2016; Hu et al., 2016).

95 However, few studies have been so far dedicated to estimate the effectiveness of the GLP in  
96 controlling air pollution on a regional scale, especially in North China Plain (NCP). In the NCP,  
97 the thermal power plants are very densely distributed, resulting in massive emissions of air  
98 pollutants (Liu et al., 2015). As a result, the GLP could produce significant energy-saving and  
99 reduce the associated air pollutant emissions from thermal power generation. Although the  
100 GLP is under the strong and sustained government commitment, however, there is no built-in  
101 mechanism for monitoring the GLP and without regularly issued official program assessment  
102 reports (Guo and Pachauri, 2017). During the past decades, the Chinese government has  
103 published only one report regarding the performance of the GLP (NDRC, 2005). There are  
104 several articles and books for summarizing the GLP from time to time by the Energy Research  
105 Institute under China's NDRC, providing additional information for assessments (Yu and Zhou,  
106 2001; Liu, 2006; Liu and Zhao, 2011; Liu, 2012; Lv and Lv, 2012; Gao and Zheng, 2016).

107 Previous studies do not well investigate the effects of the GLP on air pollution, such as the  
108 resultant of emission reductions of air pollutants, or the consequent effects on haze pollution.

109 In the present study, we quantified the effect of the GLP on the haze pollution in the NCP, a  
110 severe air polluted region in China. The study included satellite measurements and numerical  
111 model studies (WRF-CHEM). We first investigated the lighting coal consumption and



112 resultant coal-saving induced by the GLP utilizing the satellite nighttime lights (NTL) data  
113 (Elvidge et al., 2009), which has been widely used to estimate the consumption of energy and  
114 electricity (He et al., 2013; Huang et al., 2014). Then we evaluated the potential emission  
115 reductions and resultant effects on air pollution in the NCP using the WRF-CHEM model. This  
116 study provided an overall perspective on gaps of the unevaluated potential benefits to haze  
117 pollution induced by the GLP, which can inspire more macroscopic and interdisciplinary  
118 analysis in long-term national activities based on NTL datasets. We summarized the data, the  
119 methodology, and the WRF-CHEM model description in Section 2. Results and discussions  
120 were presented in Section 3, followed by the summaries and conclusions in Section 4.

## 121 **2 Data and methodology**

### 122 **2.1 The long-term NTL data and coal consumption**

123 In order to understand the spatial distributions of lighting before and after the GLP in China,  
124 we investigated the version 4 of the Defense Meteorological Satellite Program Operational  
125 Line Scanner (DMSP/OLS) NTL time series data from 1992 to 2013 (Elvidge et al., 2014).  
126 The dataset available at: <https://ngdc.noaa.gov/eog/dmsp/downloadV4composites.html>. We  
127 selected the stable light datasets, which are the cloud-free composites using all the archived  
128 DMSP/OLS smooth resolution data for calendar years. The images represent the average  
129 intensity of NTL with DN values ranging from 0 to 63 in 30 arc-second grids-cells (about 1 km  
130 spatial resolution). The 1992 and the 2013 datasets were used to investigate the different  
131 overview status of NTL before and after the GLP for long years. Considering the differences  
132 between the sensors, differences in the crossing times of the satellites, and degradation of the  
133 sensors (Elvidge et al., 2009; Elvidge et al., 2014), we inter-calibrated the NTL datasets



134 followed a second order regression model (Elvidge et al., 2014).

135 **Figure 1** shows the spatial distributions of the DMSP/OLS NTL data. We found that the  
136 lighting usages were significantly increased from 1992 to 2013, both in lighting intensity and  
137 spatial coverage, especially in the regions of eastern China, including the NCP, the Pearl River  
138 Delta, and the Yangtze River Delta. The rapid increase in the usage of lighting suggested that  
139 the generations of electricity were greatly enhanced.

140 **Figure 2** shows a long-term evolution of thermal power electricity and coal consumption for  
141 power generation. It shows that the thermal power electricity increased from 2000 (about  $10^{12}$   
142 kW h) to 2015 (about  $4 \times 10^{12}$  kW h), indicating that due to the rapid increase in the economics,  
143 the demand of electricity was largely enhanced in China. The emission of  $\text{SO}_2$  increased before  
144 2006, due to the increase of coal consumption. While after 2006, although the coal  
145 consumption still increased, the emission of  $\text{SO}_2$  started to decrease, suggesting that the  
146 desulfurization played important roles in the emission reductions from thermal power  
147 generation (Liu et al., 2016). The decrease of  $\text{NO}_x$  emission started to decrease in 2012, which  
148 was 6 year later than the decrease in  $\text{SO}_2$  emissions, suggesting that the denitrification played  
149 important roles in the emission reduction from thermal power generation after 2012 (Hu et al.,  
150 2016). Compared to the gas-phase emissions of  $\text{SO}_2$  and  $\text{NO}_x$ , the direct emission of particles  
151 ( $\text{PM}_{2.5}$ ) was relatively small (Liu et al., 2015). The large portion of gas-phase emissions from  
152 thermal power generation indicated that the most  $\text{PM}_{2.5}$  emitted from the power plants might  
153 be in the phase of secondary particles.

154 The above long-term variability of thermal power electricity and associated coal consumption  
155 for power generation was based on the situation that the GLP was conducted in China, which  
156 could produce a strong reduction for the coal burning emissions from thermal power



157 generation, such as air pollutants of SO<sub>2</sub> and NO<sub>x</sub>. These gases might have important effects  
158 on the PM<sub>2.5</sub> pollution in China, because they are important precursors for the production of  
159 particle matter (Seinfeld et al., 1998; Laurent et al., 2014). However, as the business as usual  
160 condition (i.e., without the GLP), the increased lighting demand could cause significant  
161 increase in thermal power electricity, and the associated growth of coal consumption for power  
162 generation during the past decades. This study was to assess the potential effects induced by  
163 the GLP on the severe haze pollution in the NCP (Tie et al., 2017; Long et al., 2018), and also  
164 displayed a good example to illustrate that scientific innovation can induce important benefits  
165 on environment issues. To assess the impacts of the GLP on the severe air polluted region in  
166 China, such as in the NCP, several important tools and data were used in this study, including a  
167 regional chemical/dynamical model (WRF-CHEM), satellite data (DMSP/OLS and S-NPP),  
168 and surface measurements of air pollutants.

## 169 **2.2 Description of the WRF-CHEM model**

170 We used a specific version of the WRF-CHEM model (Grell et al., 2005). The model included  
171 a new flexible gas-phase chemical module and the Models3 community multi-scale air quality  
172 (CMAQ) aerosol module developed by the US EPA (Binkowski and Roselle, 2003). The  
173 model included the dry deposition (Wesely 1989) and wet deposition followed the CMAQ  
174 method. The impacts of aerosols and clouds on the photochemistry (Li et al., 2011b) were  
175 considered by the photolysis rates calculation in the fast radiation transfer model (Tie et al.,  
176 2003; Li et al., 2005). The inorganic aerosols (Nenes et al., 1998) were predicted using the  
177 ISORROPIA Version 1.7. We also used a non-traditional secondary organic aerosol (SOA)  
178 model, including the volatility basis-set modeling approach and SOA contributions from  
179 glyoxal and methylglyoxal. Detailed information about the WRF-CHEM model can be found



180 in previous studies (Li et al., 2010; Li et al., 2011a; Li et al., 2011b; Li et al., 2012).

181 In the present study, we simulated severe haze pollution from 1 to 31 December 2015 in the

182 NCP. The domain, centered at the point of (116° E, 38° N), was composed horizontally of 300

183 by 300 grid points spaced with a resolution of 6 km (**Fig. 3**) and vertically with 35 sigma levels.

184 The physical parameterizations included the microphysics scheme (Hong and Lim 2006), the

185 Mellor–Yamada–Janjic turbulent kinetic energy planetary boundary layer scheme (Janjić,

186 2002), the unified Noah land-surface model (Chen and Dudhia, 2001), the Goddard long wave

187 radiation parameterization (Chou and Suarez, 1999), and the shortwave radiation

188 parameterization (Chou et al., 2001). Meteorological initial and boundary conditions were

189 obtained from the 1° by 1° reanalysis data of National Centers for Environmental Prediction

190 (Kalnay et al., 1996). The spin-up time of WRF-CHEM model is 3 days. The chemical initial

191 and boundary conditions were constrained from the 6 h output of Model of Ozone and Related

192 chemical Tracers, Version 4 (Horowitz et al., 2003).

193 We utilized the anthropogenic emission inventory developed by Tsinghua University (Zhang et

194 al., 2009), including anthropogenic emission sources from transportation, agriculture, industry

195 and power generation and residential. The dataset can be accessible from the website of MEIC

196 (<http://www.meicmodel.org>), providing for the community a publically accessible emission

197 dataset over China with regular updates. The emission inventory used in the present study is

198 updated and improved for the year 2015. In addition, the emissions of SO<sub>2</sub>, NO<sub>x</sub>, and CO have

199 been adjusted according to the observations during the period. Emissions from biogenic

200 sources were calculated online using the Model of Emissions of Gases and Aerosol from

201 Nature model (MEGAN) (Guenther et al. 2006).



### 202 2.3 Analysis of satellite data and model domain

203 Since the launch of the Suomi-National Polar-orbiting Partnership satellite in 2011, the  
204 Day/Night Band for the Visible Infrared Imaging Radiometer Suite (VIIRS DNB) has been  
205 widely used in recent studies, which confirmed to establish empirical relationships with energy  
206 use (Román and Stokes, 2015; Coscieme et al., 2014). To some extent, the VIIRS NTL dataset  
207 (in 15 arc-second grids-cells, about 500 m) are superior to the DMSP/OLS NTL dataset  
208 (Elvidge et al., 2013). In the present study, we used the version 1 of VIIRS NTL dataset to  
209 investigate the consumption of lighting electricity in each province, defined as provincial  
210 dynamics as follow.

$$211 \quad PD_i = \frac{\sum_i L_j \times S_j}{\sum_w L_j \times S_j} \quad (1)$$

212 where  $i$  denotes the provincial domain, and  $w$  is the nationwide domain.  $j$  is the pixel of VIIRS  
213 NTL dataset.  $S$  is the area of pixel  $j$ .  $L$  is the NTL radiance. The annual VIIRS NTL dataset  
214 contains cloud-free average of NTL radiance by excluding any data impacted by stray light,  
215 and further screening out the fires and other ephemeral lights and background (non-lights). The  
216 dataset is available at: [https://ngdc.noaa.gov/eog/viirs/download\\_dnb\\_composites.html](https://ngdc.noaa.gov/eog/viirs/download_dnb_composites.html).

217 The distribution of VIIRS NTL radiance in 2015 (**Fig. S1**) was similar as the DMSP/OLS DN  
218 values (**Fig. 1**). The high values of annual NTL radiance were concentrated in the densely  
219 populated and industrial developed areas of China (**Fig. S1a**), such as the NCP, the Yangtze  
220 River Delta, and the Pearl River Delta. There were “hot spot” located in some megacities, such  
221 as the Beijing, Tianjin, Shanghai, Guangzhou, where the NTL radiance can reach as high as 20  
222  $\text{mW}/\text{m}^2/\text{sr}$ . Statistically, 12.8% of these China’s land areas consumes 58.3% of lighting  
223 electricity consumption. The high values of provincial dynamics also concentrated on these  
224 regions, and all the provincial dynamics exceeding 5% were coastal cities (**Fig. S1b**). In the



225 NCP, in addition to the high usage of lighting, there is a large amount of power plants (Liu et  
226 al., 2015). We selected the NCP (**Fig. 3**) as the region of interest. In addition, there are  
227 extensive measurement sites of pollutants in the domain (the green crosses in **Fig. 3**).

#### 228 **2.4 Estimation of coal-saving induced by the GLP**

229 According to the analysis for the Chinese GLP program (Guo and Pachauri, 2017), the lighting  
230 activities can be defined as three clusters according to their usages: (**C<sub>1</sub>**) For outdoor lighting,  
231 such as road lights; (**C<sub>2</sub>**) household usage, mainly for residential applications; (**C<sub>3</sub>**) commercial  
232 and industrial buildings. In practice, the core of the GLP is to improve luminous efficiency,  
233 replacing low-efficiency lighting lamps by high-efficiency ones. The details of the GLP  
234 program were as follows. For **C<sub>1</sub>**, the High Pressure Sodium lamps (HPS) and Metal Halide  
235 (MH) lamps are primarily used to replace High Pressure Mercury-vapor lamps (HPM). For **C<sub>2</sub>**,  
236 the Compact Fluorescent Lamps (CFLs) are used to replace incandescent lamps (ILs). For **C<sub>3</sub>**,  
237 the T8/T5 fluorescent tubes are used to replace T12/T10 fluorescent tubes. The emerging LED  
238 lamps were not covered, however, it promotes to each of the above cluster (Pan, 2018; Wang,  
239 2017; Asolkar and Dr., 2017; Xie et al., 2016; Ge et al., 2016; Edirisinghe et al., 2016). Here  
240 the LED lamps were allocated proportionally based on the proportions of the lighting  
241 electricity consumption of **C<sub>1</sub>**, **C<sub>2</sub>**, and **C<sub>3</sub>**.

242 According to the classification above, we estimated the current equivalent luminous efficacy  
243 ( $ELE_{GLP}$ ) weighted by the proportion of their lighting electricity consumption. To investigate  
244 the potential effectiveness of the GLP, we also calculated the equivalent luminous efficacy  
245 without the implementation of the GLP ( $ELE_{no-GLP}$ ).

$$246 \quad ELE_{GLP} = \sum f_k LE_{k,GLP} \quad (2)$$

$$247 \quad ELE_{no-GLP} = \sum f_k LE_{k,no-GLP} \quad (3)$$



248 where  $k$  denotes the specified cluster of lighting lamps.  $f_k$  is the proportion of lighting  
249 electricity consumed by the  $k^{\text{th}}$  cluster lamps;  $LE_{k,GLP}$  and  $LE_{k,no-GLP}$  denote the equivalent  
250 luminous efficacy of the  $k^{\text{th}}$  cluster lamps with and without the improvement of lighting  
251 efficacy induced by the GLP. The ELE is a comprehensive parameter to reflect the lighting  
252 efficacy. In terms of current consumption levels of lighting electricity, the lighting coal  
253 consumption for power generation is proportional to ELE. As a result, the potential coal-saving  
254 induced by the GLP ( $dC$ ) can be estimated by:

$$255 \quad dC = C_0 \times \frac{ELE_{no-GLP} - ELE_{GLP}}{ELE_{GLP}} \quad (4)$$

256 where  $C_0$  denotes the current coal consumption for thermal power generation. To get the  
257 spatial distribution of potential provincial coal-savings ( $dC_i$ ), we spatially scaled the total  
258 potential coal-saving ( $dC$ ) according to the provincial dynamics factor ( $PD_i$ ), which is  
259 calculated based on the spatiotemporal dynamic of electric power consumption in each  
260 province (Elvidge et al., 1997; Chen and Nordhaus, 2011; He et al., 2013).

$$261 \quad dC_i = dC \times PD_i \quad (5)$$

262 where  $i$  denotes the province;  $PD_i$  reflects provincial dynamics of lighting coal consumption,  
263 which was explained in **Eq. 1**.

264 To estimate the emission reduction induced by the GLP, we assumed that the potential  
265 emission reduction was mainly due to the emissions from the thermal power plants. Based on  
266 the current anthropogenic emission inventory from MEIC (Multi-resolution emission inventory  
267 for China) (Liu et al., 2015; Zhang et al., 2009), the potential emission reduction ( $dE_{power,spec}$ )  
268 induced by the GLP was proportional to the associated potential coal-saving for the thermal  
269 power generation.

$$270 \quad \frac{dE_{power,spec}}{dC} = \frac{E_{power,spec}}{C_0} \quad (6)$$



271 where  $E_{power,spec}$  denotes the emission inventory from the thermal power sector;  $spec$  is the  
272 specify air pollutant of WRF-CHEM species.  $dC$  and  $C_0$  are the same as that in Eq. 4.

### 273 **2.5 WRF-CHEM sensitive studies**

274 Based on previous studies (Guo and Pachauri, 2017), the effective luminous efficacy (ELE)  
275 increased from 50 lm/W to 70–140 lm/W for  $C_1$ , from 15 lm/W to 50–60 lm/W for  $C_2$ , and  
276 from 70–80 lm/W to 80–105 lm/W for  $C_3$ . Simultaneously, the LED has experienced a fast  
277 growth since 2011, with the marketing share of LED lamps reached 32% in 2015, and the high  
278 efficacy LED lamps with 150 lm/W had been industrialized production in China (Gao and  
279 Zheng, 2016). Here we treated the marketing share of LED lamps as the proportion of its  
280 lighting electricity consumption. Then it was allocated proportionally to the clusters according  
281 to the research of Zheng et al., (2016), which reported the proportion of its lighting electricity  
282 consumption with  $C_1$ :  $C_2$ :  $C_3$  being 31.6%: 19.7%: 48.7%. More detailed information can be  
283 founded in **Table 1**.

284 The estimated ELE values have uncertainties for both low and high efficient lamps, ranging  
285 from 52.8 to 57.7 lm/W and from 96.2 to 120.9 lm/W for the ELE with or without the GLP,  
286 respectively (see **Table 1**). In addition, the estimate of lighting electricity accounts for 10–14%  
287 of the total electricity (Zheng et al., 2016; Lv and Lv, 2012). As a result, the model sensitive  
288 studies included low-limit and high-limit of electricity power savings. To account for all of the  
289 uncertain ranges, in the lower limit model simulation, the thermal power was estimated to  
290 increase 6.7%, without the GLP. In the higher limit model simulation, the thermal power was  
291 estimated to increase 18.7%, without the GLP. **Figure 4** shows that under lower and higher  
292 limit assumptions, the potential coal-savings induced by the GLP were 120–323 million tons,  
293 respectively. According to these estimates into the reference emission inventory ( $E_{0,spec}$ ), the



294 emission of pollutants, with the 3 cases (reference, low-limit, and high-limit) were estimated  
295 and shown in **Table 2**. The reference emission inventory is developed by Tsinghua University  
296 (Zhang et al., 2009), including current emission levels of thermal power plants (with  
297 considering GLP).

298 **Table 2** also shows that the direct emission of PM<sub>2.5</sub> was much smaller than the direct  
299 emission of SO<sub>2</sub> and NO<sub>x</sub> in gas-phase. The PM<sub>2.5</sub> concentrations included two different parts  
300 from thermal power plants. One was from the direct emission of PM<sub>2.5</sub> in particle phase, and  
301 the other was the secondary particle (PM<sub>2.5</sub>), which was formed from the chemical  
302 transformation from SO<sub>2</sub> and NO<sub>x</sub>. As a result, the large effect of the GLP on haze pollutions  
303 was due to the changes in the emissions of SO<sub>2</sub> and NO<sub>x</sub> from the thermal power plants.

### 304 **3 Results and discussions**

#### 305 **3.1 Model evaluation**

306 To better understand the effect of the GLP on the haze pollution in the NCP, we first  
307 conducted an evaluation of the WRF-CHEM model performance. The modeled results were  
308 compared to the hourly near-surface concentrations of CO, SO<sub>2</sub>, NO<sub>2</sub>, and PM<sub>2.5</sub>. The data was  
309 measured by the China's Ministry of Environmental Protection (MEP), and are accessible from  
310 the website <http://www.aqistudy.cn/>. The locations of the measurement sites show in **Fig. 3**.

311 The model results were evaluated by calculating the following statistical parameters, including  
312 normalized mean bias (*NMB*), the index of agreement (*IOA*), and the correlation coefficient (*r*).  
313 These parameters were used to assess the performance of REF case in simulations against  
314 measurements.

$$315 \quad NMB = \frac{\sum_{i=1}^N (P_i - O_i)}{\sum_{i=1}^N O_i} \quad (7)$$



$$IOA = 1 - \frac{\sum_{i=1}^N (P_i - O_i)^2}{\sum_{i=1}^N (|P_i - \bar{P}| + |O_i - \bar{O}|)^2} \quad (8)$$

$$r = \frac{\sum_{i=1}^N (P_i - \bar{P})(O_i - \bar{O})}{[\sum_{i=1}^N (P_i - \bar{P})^2 \sum_{i=1}^N (O_i - \bar{O})^2]^{\frac{1}{2}}} \quad (9)$$

318 where  $P_i$  and  $O_i$  are the calculated and observed air pollutant concentrations respectively.  $N$   
319 is the total number of the predictions used for comparisons.  $\bar{P}$  and  $\bar{O}$  represent the average  
320 predictions and observations, respectively. The  $IOA$  ranges from 0 to 1, with 1 showing perfect  
321 agreement of the prediction with the observation. The  $r$  ranges from -1 to 1, with 1 implicating  
322 perfect spatial consistency of observation and prediction.

323 **Figure 5** shows the temporal variation of modeled results with the measured values during  
324 December 2015. The measured values of pollutants ( $PM_{2.5}$ ,  $NO_2$ ,  $SO_2$ , and  $CO$ ) averaged in the  
325 NCP were compared with the modeled results. The results indicate that there were strong  
326 episodes of the hourly  $PM_{2.5}$  mass concentrations, with the highest values of exceeding  $300 \mu g$   
327  $m^{-3}$ , implicating that several haze events occurred during the period. There are several peak  
328 values of  $PM_{2.5}$  concentrations occurred during period, with a highest peak occurred between  
329 22-24<sup>th</sup> December. Comparing with  $CO$  temporal variability, the temporal variations between  
330  $CO$  and  $PM_{2.5}$  were similar. The modeled  $PM_{2.5}$  and  $CO$  captured the strong temporal variation,  
331 with the  $IOA$  of 0.98 and the  $NMB$  of 1.3% for  $PM_{2.5}$  mass concentrations and  $IOA$  of 0.89 and  
332 the  $NMB$  of 4.3% for  $CO$  mass concentrations. Since the  $CO$  variability was mainly  
333 determined by meteorological conditions, the similarity of the temporal variability suggested  
334 that the meteorological conditions had important contribution to the several peak values of the  
335 episode, and the model simulation well captured the meteorological conditions during the  
336 study period.

337 Although there was a similarity of the temporal variability between  $PM_{2.5}$  and  $CO$ , the  
338 magnitude of the variability of  $CO$  was smaller than variability of  $PM_{2.5}$ , suggesting that in



339 addition to the meteorological conditions, the chemical formation also played important roles  
340 for producing the high peaks of  $PM_{2.5}$  concentrations. It is important to simulate the measured  
341 temporal variations of  $SO_2$  and  $NO_x$ , because they are important chemical precursors (Seinfeld  
342 and Pandis, 1998; Laurent. et al., 2014), and are the major pollutants emitted from the thermal  
343 power plants (**Table 2**). As shown in **Fig. 5**, both the measured and modeled  $SO_2$  and  $NO_x$  had  
344 several episodes, which were corresponding to the episodes of the  $PM_{2.5}$ . The parameters  
345 between the measured and modeled results were acceptable, with the *IOA* of 0.83 and the *NMB*  
346 of 1.3% for  $SO_2$ , and *IOA* of 0.93 and the *NMB* of 6.1% for  $NO_x$ . It is interesting to note that  
347 the occurrences of the peak of  $SO_2$  and  $NO_x$  are about 1-2 days ahead of the peak of  $PM_{2.5}$ .  
348 One of the explanations was that there was chemical conversion from gas-phase of  $SO_2$  and  
349  $NO_x$  to particle phase of  $PM_{2.5}$ , resulting in the time lag between the peaks of  $SO_2$ - $NO_x$  and  
350  $PM_{2.5}$ , because  $SO_2$  and  $NO_x$  were the precursors of  $PM_{2.5}$  (Seinfeld and Pandis, 1998; Laurent.  
351 et al., 2014). As we state in the previous sections, the large effect of the GLP on haze  
352 pollutions was due to the changes in the emissions of  $SO_2$  and  $NO_x$  from the thermal power  
353 plants. The good statistical performance of the modeled  $SO_2$  and  $NO_x$  provided confident to  
354 use the model to study the GLP effects on haze in the NCP region.

355 In order to do more thoughtful validation of the model performance, **Figure 6** shows the  
356 measured and modeled spatial distributions of  $PM_{2.5}$ ,  $SO_2$ , and  $NO_x$  in the NCP. The model  
357 generally reproduced the spatial variations of  $PM_{2.5}$ ,  $NO_2$ , and  $SO_2$ , capturing the spatial  
358 characters. For example, the  $SO_2$  were largely emitted from thermal power plants and steel  
359 industrials, which were large point sources. As a result, both the modeled and measured  $SO_2$   
360 appeared as scattered distributions (see **Fig. 6d**). The correlation coefficients (*r*) between the  
361 measured and modeled results were 0.86, 0.68, and 0.70 for  $PM_{2.5}$ ,  $NO_2$ , and  $SO_2$ , respectively.



362 In general, the NCP encountered severe haze pollution events during the December 2015. The  
363 statistical analysis showed that the WRF-CHEM model reasonably captured the spatial and  
364 temporal variations of haze pollution in the NCP, although some model biases existed. The  
365 model validation provided a confident to the further model studies.

### 366 **3.2 Potential benefit of the GLP to air pollution in the NCP**

367 There are massive emissions of NO<sub>x</sub> and SO<sub>2</sub> from thermal power plants in the research  
368 domain, producing 299.1 Gg and 103.7 Gg (**Tab. 1**) during the December 2015, for NO<sub>x</sub> and  
369 SO<sub>2</sub>, respectively. There is more emission amount of NO<sub>x</sub> than SO<sub>2</sub>, because the SO<sub>2</sub>  
370 emissions from power had been significantly declined since 2005, whereas the NO<sub>x</sub> emissions  
371 were slightly declined (see **Fig. 2**) due to lower effective NO<sub>x</sub> emission control facilities (Liu  
372 et al., 2015; Huang et al., 2016).

373 According to the estimate of 6.7–18.0% of potential coal-saving induced by the GLP (**Sect.**  
374 **2.5**), the potential emission reductions from power generation were calculated base on **Eq. 6**,  
375 and the emission reductions of NO<sub>x</sub> and SO<sub>2</sub> induced by the GLP were estimated for the  
376 WRF-CHEM model sensitive studies. **Figure 7** shows the spatial distributions of changes in  
377 NO<sub>x</sub> and SO<sub>2</sub> emissions in the research domain, especially the provinces of Hebei, Henan, and  
378 Shandong within the NCP, where concentrated most of the power plants (Liu et al., 2015). The  
379 results show that under low limit estimate, without the GLP, the NO<sub>x</sub> and SO<sub>2</sub> emissions  
380 would be increased by 20.0 Gg and 6.9 Gg, respectively, in December 2015. Under high limit  
381 estimate, without the GLP, the NO<sub>x</sub> and SO<sub>2</sub> emissions would be increased by 53.8 Gg and  
382 18.7 Gg in the NCP. These large emission changes without the GLP could cause important  
383 effects on the air pollution. In the following sections, the GLP effect on the reduction of air  
384 pollution was investigated by using the WRF-CHEM model.



385 According to the lower and upper limits of emission reductions induced by the GLP, we  
386 evaluated their resultant effects on air pollutants ( $\text{PM}_{2.5}$ ,  $\text{NO}_2$ , and  $\text{SO}_2$ ), which are estimated  
387 by the difference of the SEN-GLP cases and the REF case (**Fig. 8**). The result shows that the  
388 GLP has important effects on  $\text{PM}_{2.5}$  concentrations (see **Figs 8a and 8b**), implicating the  
389 remarkable benefit to haze pollution in the NCP. In the lower limit case, the  $\text{PM}_{2.5}$   
390 concentrations could be decreased by 2–5  $\mu\text{g m}^{-3}$  in large areas within the NCP, such as the  
391 southeastern Hebei, northeastern Henan, and western Shandong (**Fig. 8a**). In the upper limit  
392 case, there is much more remarkable decrease in  $\text{PM}_{2.5}$  concentrations (4–10  $\mu\text{g m}^{-3}$ ) in wider  
393 areas within the NCP (**Fig. 8b**). We can also find large-scale reductions of  $\text{NO}_2$  and  $\text{SO}_2$  in the  
394 NCP (**Fig. 8c-f**). For example, in high limit case, the reduction of  $\text{NO}_2$  ranges from 1–8  $\mu\text{g m}^{-3}$ ,  
395 and the reduction of  $\text{SO}_2$  ranges from 1–4  $\mu\text{g m}^{-3}$ . We also display the species variations ( $\text{PM}_{2.5}$ ,  
396  $\text{NO}_2$ , and  $\text{SO}_2$ ) in **Fig. S2** within the areas with high  $\text{PM}_{2.5}$  changes induced by the GLP (see  
397 red-square in Fig. 8).

398 Although the influence of the GLP is to decrease  $\text{PM}_{2.5}$  concentrations, there were some slight  
399 increase in  $\text{PM}_{2.5}$  concentrations in north of NCP. As indicated in **Table 2**, the directly  
400 emission of  $\text{PM}_{2.5}$  was less than the gas-phase emissions of  $\text{NO}_x$  and  $\text{SO}_2$ , which suggested that  
401 the decrease of  $\text{PM}_{2.5}$  by applying the GLP was mainly due to the chemical conversions from  
402 gas-phase  $\text{NO}_x$  and  $\text{SO}_2$  to nitrate and sulfate particles (Seinfeld et al., 1998; Laurent et al.,  
403 2014). The slight increase of the  $\text{PM}_{2.5}$  concentrations may be induced by the changes in  $\text{O}_3$   
404 concentrations, because the chemical conversion from  $\text{NO}_x$  and  $\text{SO}_2$  to nitrate and sulfate  
405 requires the atmospheric oxidants like  $\text{O}_3$ . As shown in **Fig. S3**, there is slight increase of  $\text{O}_3$   
406 (1–2  $\mu\text{g m}^{-3}$ ) due to the GLP, and the slightly increase the oxidation of  $\text{SO}_2$ , which may cause  
407 some enhancement of sulfate concentrations (Wang et al., 2015a; Xue et al., 2016). Apparently,



408 the NO<sub>2</sub> reductions are more remarkable because of the more noteworthy NO<sub>x</sub> emission  
409 reductions induced by the GLP.

410 The GLP resulted in significant reduction of potential pollutant emissions from the thermal  
411 power generation, corresponding to potential benefit in alleviating haze pollution in the NCP,  
412 although with few fluctuated deteriorations. It also benefits the pollution of NO<sub>x</sub> and SO<sub>2</sub> in  
413 the NCP.

#### 414 **4 Summary**

415 For replacing low-efficiency lighting lamps by high-efficiency ones, the Green Lights Program  
416 (GLP) is a national energy conservation activity for saving lighting electricity consumption in  
417 China, resulting in an effective reduction of coal consumption for power generation. However,  
418 despite of the great success of the GLP in lighting electricity, the effects of the GLP on haze  
419 pollution are not investigated and well understood. In the present study, we try to assess the  
420 potential coal-saving induced by the GLP, and to estimate its resultant benefit to the haze  
421 pollutions in the NCP, China, where often suffer from severe haze pollutions. First, we used  
422 the satellite dataset of nighttime lights to evaluate the associated saving of lighting electricity  
423 consumption and its resultant coal-saving in the NCP. Second, we estimated the emission  
424 reductions from thermal power generation induced by the GLP, based on the emission  
425 inventory developed by Tsinghua University (Zhang et al., 2009). Finally, we applied the  
426 WRF-CHEM model to evaluate the potential effects of the GLP on the haze pollutions in the  
427 NCP. The model results had been evaluated by a comparison with surface measurements. And  
428 two sensitivity experiments were conducted to explore the role of the GLP in benefiting the  
429 haze pollution. Some important results are summarized as follows.

430 1. Due to the rapid increase in the economics, the demand of electricity is largely enhanced in



431 China. As a result, the thermal power electricity increase from 2000 (about  $10^{12}$  kW h) to  
432 2015 (about  $4 \times 10^{12}$  kW h), suggesting that the lighting electricity consumption could  
433 produce higher emissions of air pollutions in the densely populated and industrial developed  
434 regions of China.

435 2. The GLP program significantly improves in lighting efficiency by 66.8–128.8%,  
436 implicating 6.7–18.0% of potential savings for electricity consumption, as well as potential  
437 coal-savings in thermal power generation.

438 3. The estimated potential coal-saving induced by the GLP can reach a massive value of 120–  
439 323 million tons, accounting for 6.7–18.0% of the total coal consumption for thermal power  
440 generation in China. As a result, there is a massive potential emission reduction of air  
441 pollutants from thermal power generation, involving 20.0–53.8 Gg for NO<sub>x</sub> and 6.9–18.7  
442 Gg for SO<sub>2</sub> in the NCP of China. The reductions of these emissions play important roles in  
443 reducing the haze formation in the NCP, because NO<sub>x</sub> and SO<sub>2</sub> are important precursors for  
444 the particles.

445 4. The reduction of NO<sub>x</sub> and SO<sub>2</sub> from power plants produces a remarkable benefit to haze  
446 pollution in the NCP. The sensitive studies by using the WRF-CHEM model shows that the  
447 GLP has important effects on PM<sub>2.5</sub> concentrations in the NCP. In the lower limit case, the  
448 PM<sub>2.5</sub> concentrations could be decreased by 2–5  $\mu\text{g m}^{-3}$  in large areas within the NCP. In the  
449 upper limit case, there is much more remarkable decrease in PM<sub>2.5</sub> concentrations (4–10  $\mu\text{g}$   
450  $\text{m}^{-3}$ ) in wider areas within the NCP.

451 This study is a good example to illustrate that scientific innovation can induce important  
452 benefits on environment issues, such as haze pollution.

453



454 **Author contributions**

455 X. T., and X. L. designed the study. X.-K. L. provided measurement data. J.-M.Z., W.-T. D.,  
456 F. T., G.-H. L. analyzed the data. X. L. and X. T. wrote the manuscript. J. C. and Z. A.  
457 overviewed the paper. All authors commented on the manuscript.

458

459 **Acknowledgement**

460 This work is supported by the National Natural Science Foundation of China (NSFC) under  
461 Grant No. 41430424 and 41730108, and the Ministry of Science and Technology of China  
462 under Grant No. 2016YFC0203400. The National Center for Atmospheric Research is  
463 sponsored by the National Science Foundation.

464 **Reference**

- 465 Asolkar, K., and Dr., A. S. S.: Energy Efficient Intelligent Household LED Lighting System  
466 Based On Daylight Illumination, *Int. J. Eng. Tech.*, 9, 4258-4264, 2017.
- 467 Binkowski, F. S., and Roselle, S. J.: Models - 3 Community Multiscale Air Quality (CMAQ)  
468 model aerosol component 1. Model description, *J. Geophys. Res.*, 108, 2003.
- 469 Chen, F., and Dudhia, J.: Coupling an advanced land surface–hydrology model with the Penn  
470 State–NCAR MM5 modeling system. Part II: Preliminary model validation, *Mon. Weather  
471 Rev.*, 129, 587-604, 2001.
- 472 Chen, X., and Nordhaus, W. D.: Using luminosity data as a proxy for economic statistics, *P.  
473 Nat. Acad. Sci. USA*, 108, 8589-8594, 2011.
- 474 Chou, M. D., and Suarez, M. J.: A solar radiation parameterization for atmospheric studies,  
475 NASA TM-104606, Nasa Tech.memo, 15, 1999.
- 476 Chou, M. D., Suarez, M. J., Liang, X. Z., Yan, M. H., and Cote, C.: A Thermal Infrared  
477 Radiation Parameterization for Atmos. Stud., *Max J*, 2001.
- 478 Coscieme, L., Pulselli, F. M., Bastianoni, S., Elvidge, C. D., Anderson, S., and Sutton, P. C.: A  
479 Thermodynamic Geography: Night-Time Satellite Imagery as a Proxy Measure of Emergy,  
480 *Ambio*, 43, 969-979, 2014.
- 481 Edirisinghe, K., Abeyweera, R., and Senanayake, N. S.: Evaluation of Effectiveness of LED  
482 Lighting in Buildings, 2016.



- 483 Elvidge, C. D., Baugh, K. E., Kihn, E. A., Kroehl, H. W., Davis, E. R., and Davis, C. W.:  
484 Relation between satellite observed visible-near infrared emissions, population, economic  
485 activity and electric power consumption, *Int. J. Remote Sens.*, 18, 1373-1379, 1997.
- 486 Elvidge, C. D., Sutton, P. C., Ghosh, T., Tuttle, B. T., Baugh, K. E., Bhaduri, B., and Bright, E.:  
487 A global poverty map derived from satellite data, *Comput. Geosci.*, 35, 1652-1660, 2009.
- 488 Elvidge, C. D., Baugh, K. E., Zhizhin, M., and Hsu, F. C.: Why VIIRS data are superior to  
489 DMSP for mapping nighttime lights, *P. Asia-Pac. Adv. Netw.*, 35, 62-69, 2013.
- 490 Elvidge, C. D., Hsu, K. E., Baugh, K., and Ghosh, T.: National Trends in Satellite Observed  
491 Lighting: 1992-2012, *Global Urban Monitoring and Assessment Through Earth Observation*,  
492 Boca Raton, FL, USA, 2014,
- 493 Gao, F., and Zheng, B.: Review of Development and Implementation of the Green Lighting  
494 Project in China, *China Illum. Eng. J.*, 2016.
- 495 Ge, A., Shu, H., Chen, D., Cai, J., Chen, J., and Zhu, L.: Optical design of a road lighting  
496 luminaire using a chip-on-board LED array, *Lighting Res. Technol.*, 49, 2016.
- 497 Grell, G. A., Peckham, S. E., Schmitz, R., McKeen, S. A., Frost, G., Skamarock, W. C., and  
498 Eder, B.: Fully coupled “online” chemistry within the WRF model, *Atmos. Environ.*, 39,  
499 6957-6975, 2005.
- 500 Guenther, A., Karl, T., Harley, P., Wiedinmeyer, C., Palmer, P. I., and Geron, C.: Estimates of  
501 global terrestrial isoprene emission using MEGAN, *Atmos. Chem. Phys.*, 6, 3181-3210, 2006.
- 502 Guo, F., and Pachauri, S.: China's Green Lights Program: A review and assessment, *Energ.*  
503 *Policy*, 110, 31-39, 2017.
- 504 He, C., Ma, Q., Liu, Z., and Zhang, Q.: Modeling the spatiotemporal dynamics of electric  
505 power consumption in Mainland China using saturation-corrected DMSP/OLS nighttime stable  
506 light data, *Int. J. Digit. Earth*, 10.1080/17538947.2013.822026, 2013.
- 507 Hong, S.-Y., and Lim, J.-O. J.: The WRF Single-Moment 6-Class Microphysics Scheme  
508 (WSM6), *Asia-Pac. J. Atmos. Sci.*, 42, 129-151, 2006.
- 509 Horowitz, L. W., Walters, S., Mauzerall, D. L., Emmons, L. K., Rasch, P. J., Granier, C., Tie,  
510 X., Lamarque, J. F., Schultz, M. G., and Tyndall, G. S.: A global simulation of tropospheric  
511 ozone and related tracers: Description and evaluation of MOZART, version 2, *J. Geophys. Res.*  
512 *Atmos.*, 108, ACH 16-11, 2003.
- 513 Hu, J., Huang, L., Chen, M., He, G., and Zhang, H.: Impacts of power generation on air quality  
514 in China—Part II: Future scenarios, *Resour. Conserv. Recy.*, 121, 115–127, 2016.
- 515 Huang, L., Hu, J., Chen, M., and Zhang, H.: Impacts of power generation on air quality in  
516 China—part I: An overview, *Resour. Conserv. Recy.*, 2016.
- 517 Huang, Q., Yang, X., Gao, B., Yang, Y., and Zhao, Y.: Application of DMSP/OLS Nighttime  
518 Light Images: A Meta-Analysis and a Systematic Literature Review, *Remote Sens.*, 6,  
519 6844-6866, 2014.
- 520 Janjić, Z. I.: Nonsingular implementation of the Mellor–Yamada level 2.5 scheme in the NCEP  
521 Meso model, NCEP office note, 437, 61, 2002.
- 522 Kalnay, E., Kanamitsu, M., Kistler, R., Collins, W., Deaven, D., Gandin, L., Iredell, M., Saha,  
523 S., White, G., and Woollen, J.: The NCEP/NCAR 40-Year Reanalysis Project,



- 524 Bull. amer. meteor Soc, 77, 437-472, 1996.
- 525 Laurent, O., Hu, J., Li, L., Cockburn, M., Escobedo, L., Kleeman, M. J., and Wu, J.: Sources  
526 and contents of air pollution affecting term low birth weight in Los Angeles County, California,  
527 2001-2008, Environ. Res., 134, 488-495, 2014.
- 528 Li, G., Zhang, R., Fan, J., and Tie, X.: Impacts of black carbon aerosol on photolysis and  
529 ozone, J. Geophys. Res., 110, 2005.
- 530 Li, G., Lei, W., Zavala, M., Volkamer, R., Dusanter, S., Stevens, P., and Molina, L.: Impacts  
531 of HONO sources on the photochemistry in Mexico City during the MCMA-2006/MILAGO  
532 Campaign, Atmos. Chem. Phys., 10, 6551-6567, 2010.
- 533 Li, G., Bei, N., Tie, X., and Molina, L.: Aerosol effects on the photochemistry in Mexico City  
534 during MCMA-2006/MILAGRO campaign, Atmos. Chem. Phys., 11, 5169-5182, 2011a.
- 535 Li, G., Zavala, M., Lei, W., Tsimpidi, A., Karydis, V., Pandis, S. N., Canagaratna, M., and  
536 Molina, L.: Simulations of organic aerosol concentrations in Mexico City using the  
537 WRF-CHEM model during the MCMA-2006/MILAGRO campaign, Atmos. Chem. Phys., 11,  
538 3789-3809, 2011b.
- 539 Li, G., Lei, W., Bei, N., and Molina, L.: Contribution of garbage burning to chloride and PM  
540 2.5 in Mexico City, Atmos. Chem. Phys., 12, 8751-8761, 2012.
- 541 Lin, J.: China green lights program: A review and recommendations, Lawrence Berkeley  
542 National Laboratory, 1999.
- 543 Liu, F., Zhang, Q., Tong, D., Zheng, B., Li, M., Huo, H., and He, K. B.: High-resolution  
544 inventory of technologies, activities, and emissions of coal-fired power plants in China from  
545 1990 to 2010, Atmos. Chem. Phys., 15, 18787-18837, 2015.
- 546 Liu, H.: China's Green Lights Program: review of the past ten years and prospect, Energ.  
547 China, 28, 17-20, 2006.
- 548 Liu, H.: The concept and practice of green lights, China Electric Power Press, 2009.
- 549 Liu, H., and Zhao, J. P.: The Implementation Manual of China Green Lights, China Environ.  
550 Sci. Press, Beijing, 2011.
- 551 Liu, H.: China's Green Lights Program in the past 20 years, J. China Illum. Eng., 23, 12-17,  
552 2012.
- 553 Long, X., Bei, N., Wu, J., Li, X., Feng, T., Xing, L., Zhao, S., Cao, J., Tie, X., An, Z., and Li,  
554 G.: Does afforestation deteriorate haze pollution in Beijing–Tianjin–Hebei (BTH), China?,  
555 Atmos. Chem. Phys., 18, 10869-10879, [10.5194/acp-18-10869-2018](https://doi.org/10.5194/acp-18-10869-2018), 2018.
- 556 Lv, F., and Lv, W. B.: The Progress and Prospect of Green Lights Program in China, China  
557 Illum. Eng. J., 23, 1-6, 2012.
- 558 NBS, National Bureau of Statistics, China Statistical Yearbook 2000-2016, China Statistics  
559 Press, Beijing, available at: <http://www.stats.gov.cn/tjsj/ndsj/>
- 560 NDRC, National Development and Reform Commission of China, 2005. China Green Lights  
561 Development Report (2004). China Elect. Pow. Press, Beijing.
- 562 Nenes, A., Pandis, S. N., and Pilinis, C.: ISORROPIA: A new thermodynamic equilibrium  
563 model for multiphase multicomponent inorganic aerosols, Aquat. geochem., 4, 123-152, 1998.



- 564 Pan, Y.: Actual Effect Tracking and Analysis of a LED Road Lighting Upgrading Project,  
565 China Light & Lighting, 2018.
- 566 Román, M. O., and Stokes, E. C.: Holidays in lights: Tracking cultural patterns in demand for  
567 energy services, *Earth. Future*, 3, 182-205, 2015.
- 568 SCIO, State Council Information Office of China, 2006. NDRC press conference on Green  
569 Lights Program. Available from:  
570 <http://www.scio.gov.cn/xwfbh/gbwxwfbh/xwfbh/fzggw/document/313370/313370.htm>, last  
571 accessed on September 5, 2018
- 572 Seinfeld, J. H., Pandis, S. N., and Noone, K.: Atmospheric Chemistry and Physics: From Air  
573 Pollution to Climate Change, *Environ. Sci. Policy Sust. Dev.*, 40, 26-26, 1998.
- 574 Tie, X., Brasseur, G., Emmons, L., Horowitz, L., and Kinnison, D.: Effects of aerosols on  
575 tropospheric oxidants: A global model study, *J. Geophys. Res. Atmos.*, 106, 22931-22964,  
576 2001.
- 577 Tie, X., Madronich, S., Walters, S., Zhang, R., Rasch, P., and Collins, W.: Effect of clouds on  
578 photolysis and oxidants in the troposphere, *J. Geophys. Res.*, 108, 2003.
- 579 Tie, X., and Cao, J.: Aerosol pollution in China: Present and future impact on environment,  
580 *Particuology*, 8, 426-431, 2010.
- 581 Tie, X., Huang, R. J., Cao, J., Zhang, Q., Cheng, Y., Su, H., Chang, D., Pöschl, U., Hoffmann,  
582 T., and Dusek, U.: Severe Pollution in China Amplified by Atmospheric Moisture, *Sci. Rep.*, 7,  
583 15760, 2017.
- 584 Wang, S., and Hao, J.: Air quality management in China: Issues, challenges, and options, *J.*  
585 *Environ. Sci.*, 24, 2-13, 2012.
- 586 Wang, Y., Zhang, Q., Jiang, J., Zhou, W., Wang, B., He, K., Duan, F., Zhang, Q., Philip, S.,  
587 and Xie, Y.: Enhanced sulfate formation during China's severe winter haze episode in January  
588 2013 missing from current models, *J. Geophys. Res. Atmos.*, 119, 10,425-410,440, 2015a.
- 589 Wang, Y. J.: Study on energy saving technology of urban road lighting LED street lighting,  
590 Heilongjiang Science, 2017.
- 591 Wang, Z., Pan, L., Li, Y., Zhang, D., Ma, J., Sun, F., Xu, W., and Wang, X.: Assessment of air  
592 quality benefits from the national pollution control policy of thermal power plants in China: A  
593 numerical simulation, *Atmos. Environ.*, 106, 288-304, 2015b.
- 594 Wesely, M.: Parameterization of surface resistances to gaseous dry deposition in regional-scale  
595 numerical models, *Atmos. Environ.*, 23, 1293-1304, 1989.
- 596 Xie, Y., Yang, Y., and Polytechnic, F.: Discussion on the application of LED lighting power  
597 drive technology, *Electron. Test*, 2016.
- 598 Xue, J., Yuan, Z., Griffith, S. M., Yu, X., Lau, A. K. H., and Yu, J. Z.: Sulfate Formation  
599 Enhanced by a Cocktail of High NO<sub>x</sub>, SO<sub>2</sub>, Particulate Matter, and Droplet pH during  
600 Haze-Fog Events in Megacities in China: An Observation-Based Modeling Investigation,  
601 *Environ. Sci. Technol.*, 50, 7325, 2016.
- 602 Yu, C., and Zhou, D.: Evaluation of the implementation of China's green lights program,  
603 *Energy China*, 2, 8-11, 2001.
- 604 Zhang, H., Li, J., Qi, Y., Jian, Z. Y., Wu, D., Yuan, C., He, K., and Jiang, J.: Source



- 605 apportionment of PM 2.5 nitrate and sulfate in China using a source-oriented chemical  
606 transport model, Atmos. Environ., 62, 228-242, 2012.
- 607 Zhang, Q., Streets, D. G., Carmichael, G. R., He, K., Huo, H., Kannari, A., Klimont, Z., Park,  
608 I., Reddy, S., and Fu, J.: Asian emissions in 2006 for the NASA INTEX-B mission, Atmos.  
609 Chem. Phys., 9, 5131-5153, 2009.
- 610 Zhao, Y., Zhang, J., and Nielsen, C. P.: The effects of recent control policies on trends in  
611 emissions of anthropogenic atmospheric pollutants and CO<sub>2</sub> in China, Atmos. Chem. Phys., 13,  
612 487-508, 10.5194/acp-13-487-2013, 2013.
- 613 Zheng, B., Gao, F., and Guo, X.: Survey Analysis of Lighting Power Consumption in China,  
614 China Light & Lighting, 2016.
- 615



616 **Tab.1**

617

618 **Table 1.** Effective Luminous Efficacy (ELE) with and without the GLP

	Cluster <sup>a</sup>	Lamp type	LE <sup>a</sup>	P <sup>b</sup>	ELE
Low-efficiency lamps					<i>ELE<sub>no-GLP</sub></i>
Lower range	C1	HPM	50 <sup>a</sup>	31.6% <sup>b</sup>	52.8
	C2	ILs	15 <sup>a</sup>	19.7% <sup>b</sup>	
	C3	T12/T10	70	48.7% <sup>b</sup>	
Upper range	C1	HPM	50 <sup>a</sup>	31.6% <sup>b</sup>	57.7
	C2	ILs	15 <sup>a</sup>	19.7% <sup>b</sup>	
	C3	T12/T10	80 <sup>a</sup>	48.7% <sup>b</sup>	
High-efficiency lamps					<i>ELE<sub>GLP</sub></i>
Lower range	C1, C2, C3	LED	150 <sup>c</sup>	32.0% <sup>c</sup>	96.2
	C1	HPS/MH	70 <sup>a</sup>	21.5% <sup>d</sup>	
	C2	CFLs	50 <sup>a</sup>	13.4% <sup>c</sup>	
	C3	T8/T5	80 <sup>a</sup>	33.1% <sup>c</sup>	
Upper range	C1, C2, C3	LED	150 <sup>c</sup>	32.0% <sup>c</sup>	120.9
	C1	HPS/MH	140 <sup>a</sup>	21.5% <sup>d</sup>	
	C2	CFLs	60 <sup>a</sup>	13.4% <sup>c</sup>	
	C3	T8/T5	105 <sup>a</sup>	33.1% <sup>c</sup>	

619 P: the proportion of lighting electricity consumed by specific cluster lamps to the total lighting electricity  
 620 consumption

621 a. The values were taken from Guo et al. (2017).

622 b. The values were taken from Zheng et al. 2016

623 c. The values were evaluated based on Gao et al., 2016

624 d. The values were estimated based on Zheng et al., 2016 and Ding et al., 2017

625 e. The values were estimated based on Refs of a, b, c, and d.

626

627 LE and ELE: (lm/W)

628 LED: light-emitting diode

629 HPM lamps: High Pressure Mercury-vapor lamps

630 HPS lamps: High Pressure Sodium lamps

631 ILs: Incandescent lamps

632 T12/T10: T12/T10 fluorescent tubes

633 C1: outdoor lighting, such as road lights

634 C2: residential applications, such as households

635 C3: commercial and industrial buildings

636

637

638 **Tab.2**

639

640 **Table 2.** Coal consumptions, and emissions for the reference case (REF), the limit cases of low  
641 (SEN-GLP-low) and high (SEN-GLP-high)

642

Species	REF (100%)	SEN-GLP-low (+6.7%)	SEN-GLP-high (+18.0%)
Coal consumption for coal-fired power in China in 2015 (Tg)			
	1793.2	119.7	323.3
Emissions from power in 3 cases in the domain in Dec. 2015 (Gg)			
NO <sub>x</sub>	299.1	299.1+20.0	299.1+53.8
SO <sub>2</sub>	103.7	103.7+6.9	103.7+18.7
PM <sub>2.5</sub>	31.1	31.1+2.1	31.1+5.6
Others	X	106.7X%	118.0X%

643

644



645

**Figure Captions**

646 **Figure 1.** The spatial distributions of the Nighttime-light data (NLT) from DMSP/OLS DN  
647 values in (a) 1992 and in (b) 2013.

648 **Figure 2.** Coal-fired power electricity and associated coal consumption for power generation,  
649 and the emissions of NO<sub>x</sub>, SO<sub>2</sub>, and PM<sub>2.5</sub> from thermal power plants from 2000 to  
650 2015 in China.

651 **Figure 3.** The horizontal domain of the model (WRF-CHEM), with the location of sampling  
652 sites (shown by the green crosses), and topographical conditions of the NCP, which  
653 are surrounded by the Mountains of Yan and Tai in the north and west, respectively.

654 **Figure 4.** The (a) lower and (b) upper limits of potential coal-savings induced by the GLP.

655 **Figure 5.** The temporal variations of predicted (red lines) and observed (black dots) profiles of  
656 near-surface mass concentrations of PM<sub>2.5</sub>, NO<sub>2</sub>, SO<sub>2</sub>, and CO averaged over all  
657 ambient monitoring sites in the NCP during December 2015.

658 **Figure 6.** The spatial comparisons of predicted and observed episode-average mass  
659 concentrations of PM<sub>2.5</sub>, NO<sub>2</sub>, and SO<sub>2</sub>. (a) Statistical comparison of predicted and  
660 observed mass concentrations, with the correlation coefficient (*r*). Horizontal  
661 distributions of predictions (color contour) and observations (colored circles) of (b)  
662 PM<sub>2.5</sub>, (c) NO<sub>2</sub>, and (d) SO<sub>2</sub>, along with the simulated wind fields (black arrows).

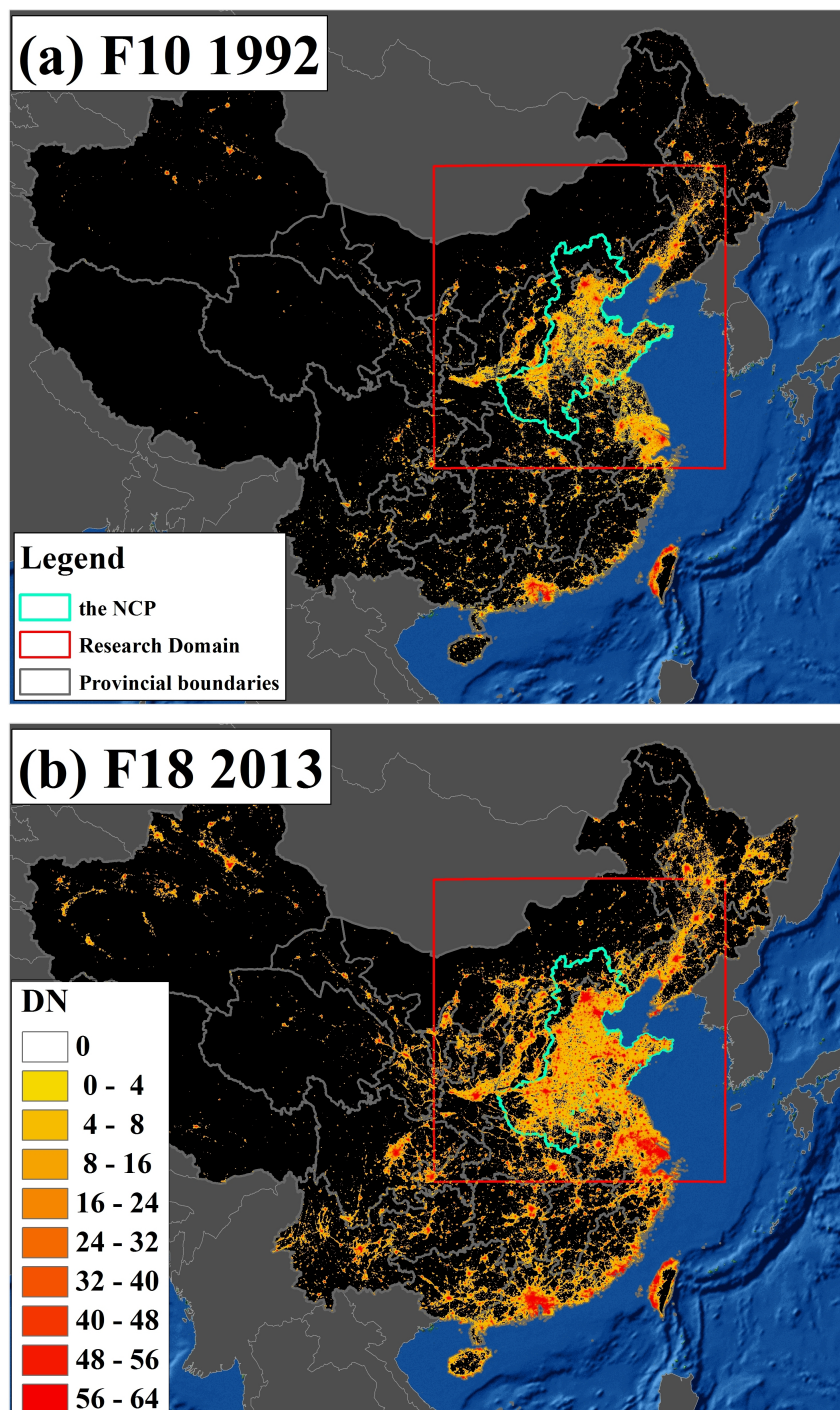
663 **Figure 7.** The potential emission reductions for low (left panels) and high (right panels) limit  
664 cases induced by the GLP, including the mass rates change of (a) NO<sub>x</sub>, and (b) SO<sub>2</sub>.  
665 The total emission reductions are also shown in the rectangle.

666 **Figure 8.** The lower (left panels) and upper (right panels) episode-averaged variations induced  
667 by GLP, including the mass concentrations (μg m<sup>-3</sup>) of (a) PM<sub>2.5</sub>, (b) NO<sub>2</sub>, and (c)  
668 SO<sub>2</sub>. The results refer to the spatial variations between the REF case and the  
669 SEN-GLPs case (REF – SNE-GLPs).

670



671 Fig. 1

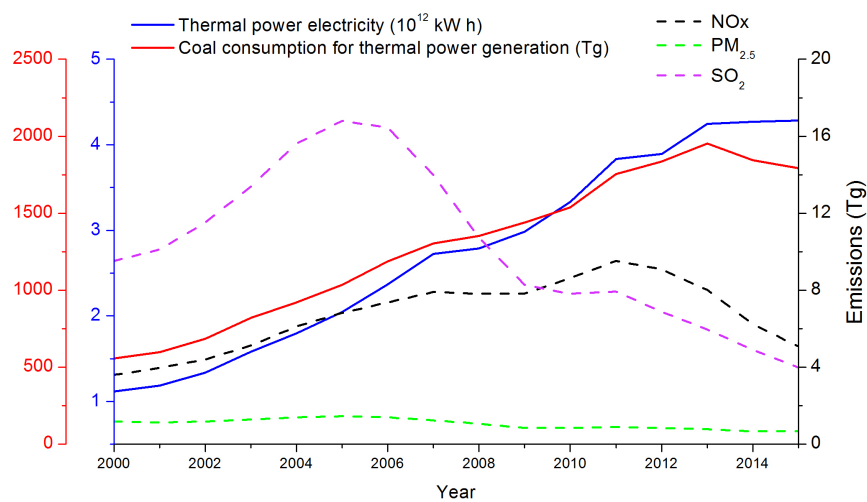


672

673 **Figure 1.** The spatial distributions of the Nighttime-light data (NLT) from DMSP/OLS DN  
674 values in (a) 1992 and in (b) 2013.



675 **Fig. 2**



676

677 **Figure 2.** Coal-fired power electricity and associated coal consumption for power generation,  
678 and the emissions of NO<sub>x</sub>, SO<sub>2</sub>, and PM<sub>2.5</sub> from thermal power plants from 2000 to 2015 in  
679 China.

680

681



682 **Fig. 3**



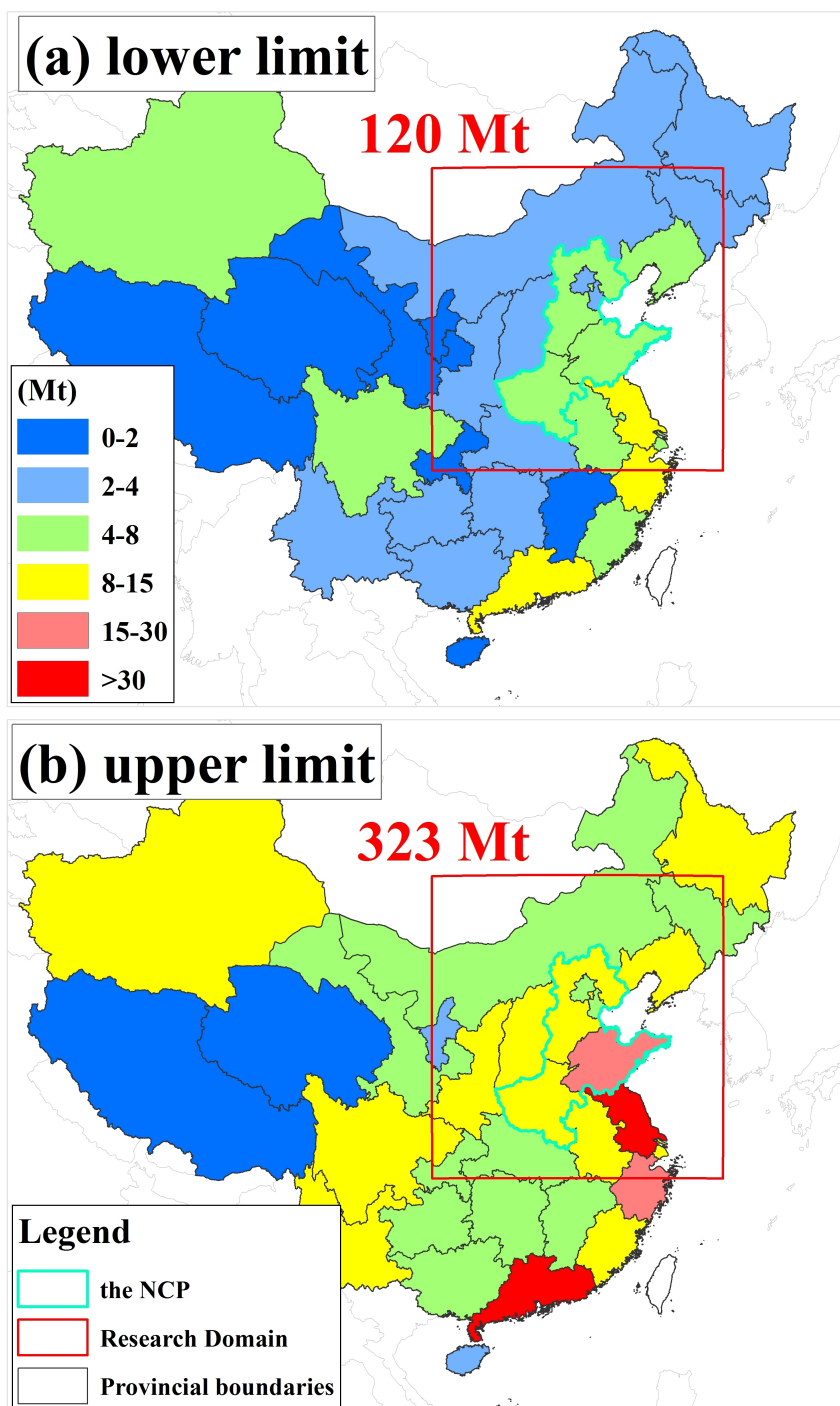
683

684 **Figure 3.** The horizontal domain of the model (WRF-CHEM), with the location of sampling  
685 sites (shown by the green crosses), and topographical conditions of the NCP, which are  
686 surrounded by the Mountains of Yan and Tai in the north and west, respectively.

687



688 Fig. 4

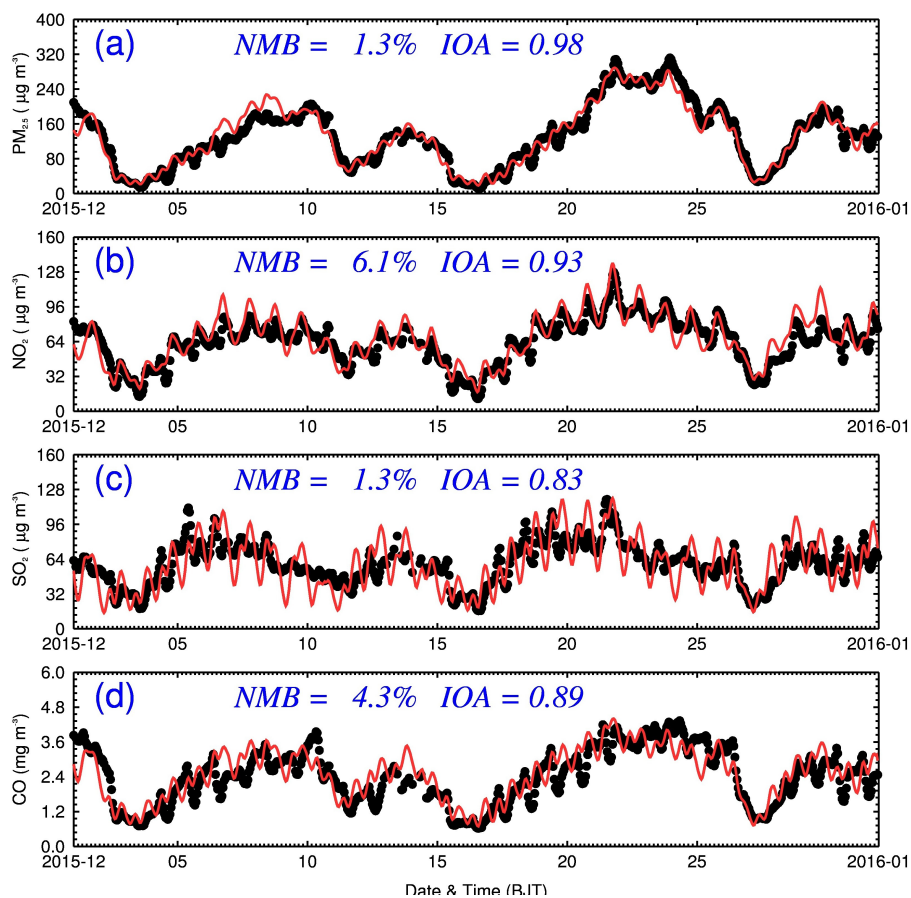


689

690 **Figure 4.** The (a) lower and (b) upper limits of potential coal-savings induced by the GLP.



691 **Fig. 5**



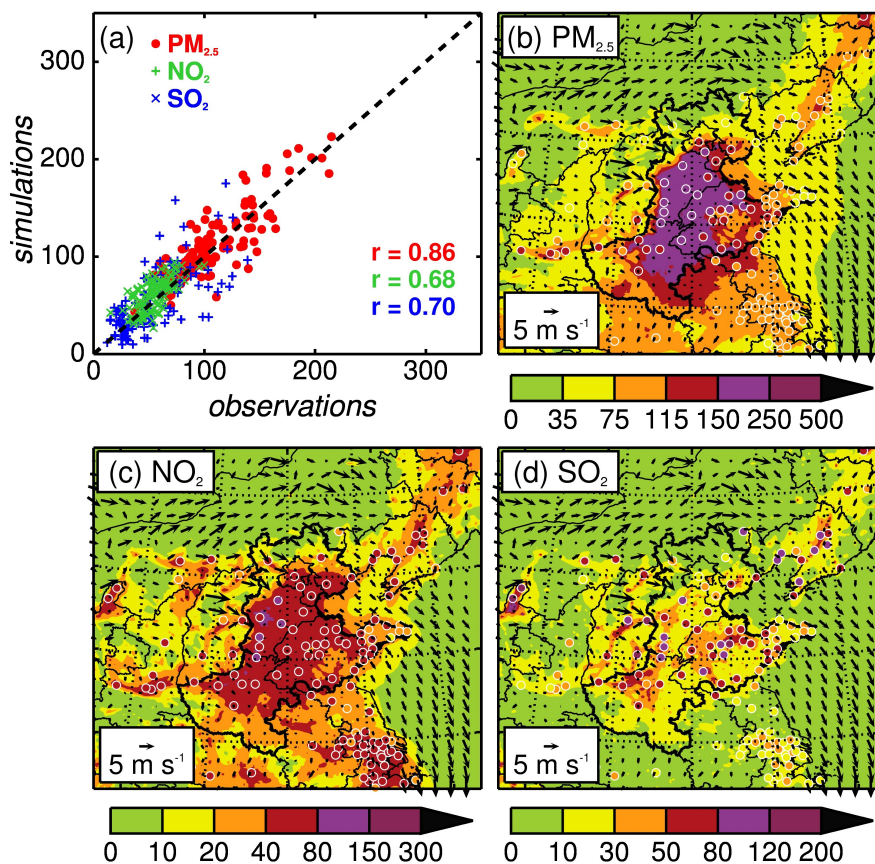
692

693 **Figure 5.** The temporal variations of predicted (red lines) and observed (black dots) profiles of  
694 near-surface mass concentrations of  $\text{PM}_{2.5}$ ,  $\text{NO}_2$ ,  $\text{SO}_2$ , and  $\text{CO}$  averaged over all ambient  
695 monitoring sites in the NCP during December 2015.

696



697 **Fig. 6**

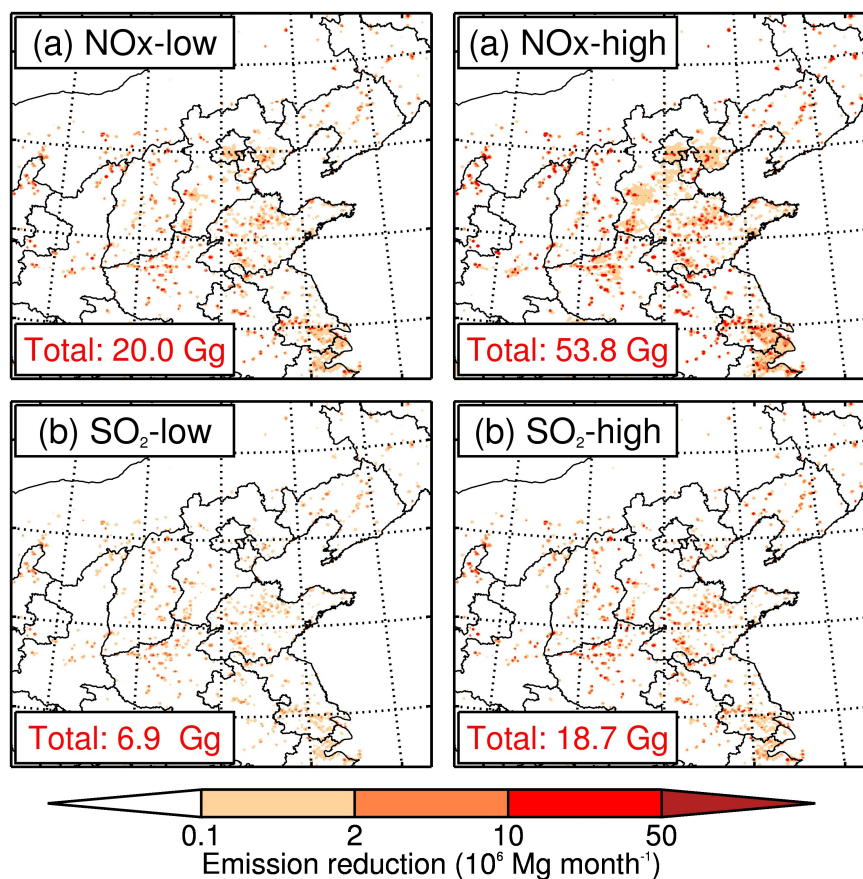


698

699 **Figure 6.** The spatial comparisons of predicted and observed episode-average mass  
700 concentrations of PM<sub>2.5</sub>, NO<sub>2</sub>, and SO<sub>2</sub>. (a) Statistical comparison of predicted and observed  
701 mass concentrations, with the correlation coefficient ( $r$ ). Horizontal distributions of predictions  
702 (color contour) and observations (colored circles) of (b) PM<sub>2.5</sub>, (c) NO<sub>2</sub>, and (d) SO<sub>2</sub>, along  
703 with the simulated wind fields (black arrows).



704 **Fig. 7**

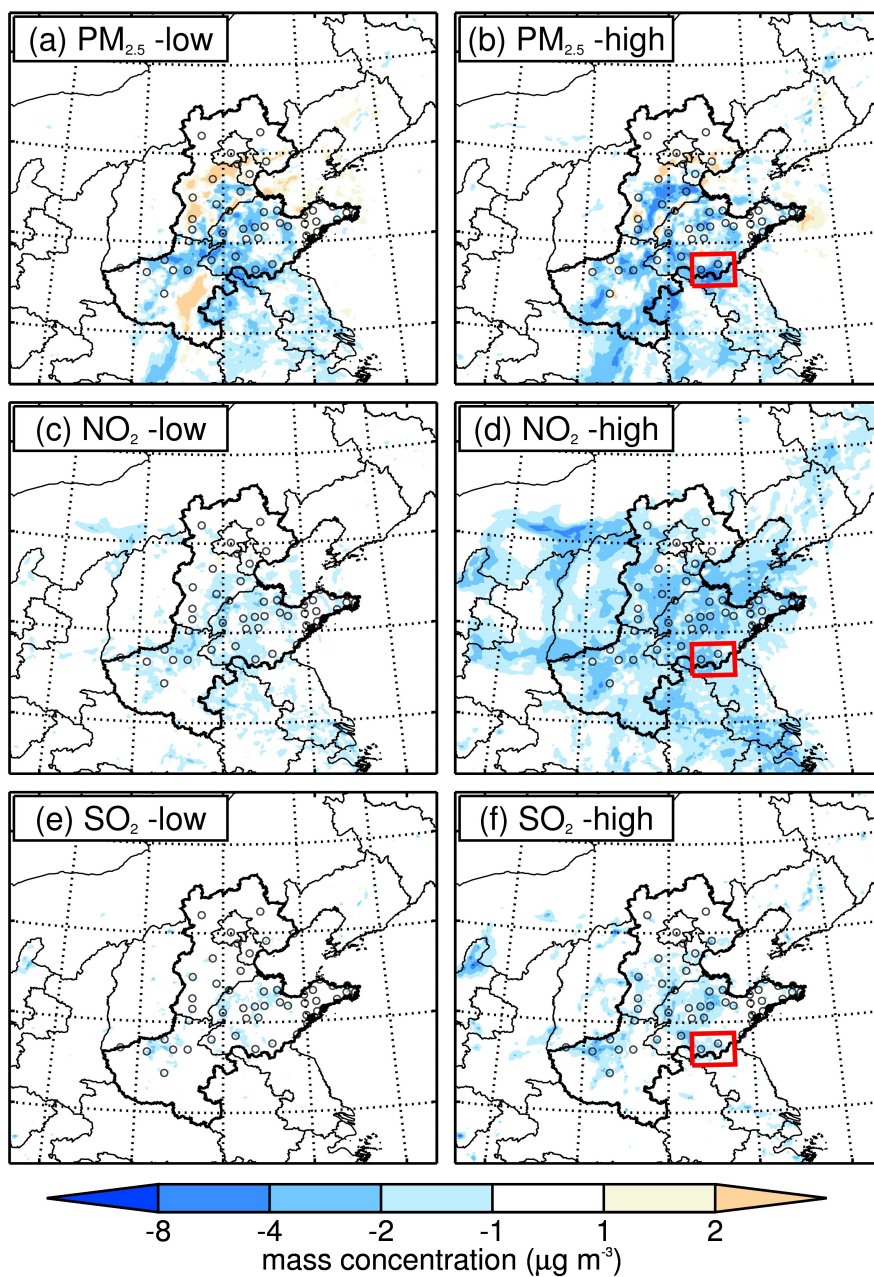


705

706 **Figure 7.** The potential emission reductions for low (left panels) and high (right panels) limit  
707 cases induced by the GLP, including the mass rates change of (a) NO<sub>x</sub>, and (b) SO<sub>2</sub>. The total  
708 emission reductions are also shown in the rectangle.



709 **Fig. 8**



710

711 **Figure 8.** The lower (left panels) and upper (right panels) episode-averaged variations induced  
712 by GLP, including the mass concentrations ( $\mu\text{g m}^{-3}$ ) of (a)  $\text{PM}_{2.5}$ , (b)  $\text{NO}_2$ , and (c)  $\text{SO}_2$ . The  
713 results refer to the spatial variations between the REF case and the SEN-GLPs case (REF –  
714 SNE-GLPs). The red-squares display the areas with high  $\text{PM}_{2.5}$  changes induced by the GLP.